

# Nonstatistical dynamics on potentials exhibiting reaction path bifurcations and valley-ridge inflection points

Peter Collins

*School of Mathematics*

*University of Bristol*

*Bristol BS8 1TW*

*United Kingdom*

Barry K. Carpenter\*

*School of Chemistry*

*Cardiff University*

*Cardiff*

*CF10 3AT*

*United Kingdom*

Gregory S. Ezra<sup>†</sup>

*Department of Chemistry and Chemical Biology*

*Baker Laboratory*

*Cornell University*

*Ithaca, NY 14853*

*USA*

Stephen Wiggins<sup>‡</sup>

*School of Mathematics*

*University of Bristol*

*Bristol BS8 1TW*

*United Kingdom*

(Dated: March 22, 2022)

## Abstract

We study reaction dynamics on a model potential energy surface exhibiting post-transition state bifurcation in the vicinity of a valley ridge inflection point. We compute fractional yields of products reached after the VRI region is traversed, both with and without dissipation. It is found that apparently minor variations in the potential lead to significant changes in the reaction dynamics. Moreover, when dissipative effects are incorporated, the product ratio depends in a complicated and highly non-monotonic fashion on the dissipation parameter. Dynamics in the vicinity of the VRI point itself play essentially no role in determining the product ratio, except in the highly dissipative regime.

PACS numbers: 34.10.+ , 82.20.-w, 82.20.D, 82.20.W

## I. INTRODUCTION

Much recent experimental and theoretical work has focussed on recognizing and understanding the manifestations of nonstatistical dynamics in thermal reactions of organic molecules (for reviews, see refs 1–7; see also the representative refs 8–19). Such research has convincingly demonstrated that, for an ever-growing number of cases, standard transition state theory (TST) and RRKM approaches<sup>20–27</sup> for prediction of rates, product ratios, stereospecificity and isotope effects can fail completely. This work is changing the basic textbook paradigms of physical organic chemistry (cf. ref. 4, Ch. 7).

While absolute rates are usually controllable with changes of temperature, relative rates (i.e., *selectivity*) often are not<sup>28</sup>. Hence, understanding the factors that control selectivity is of essential importance for synthesis, especially if existing models used for analyzing the problem are incomplete or inapplicable.

A fundamental dynamical assumption underlying conventional statistical theories of reaction rates and selectivities is the existence of intramolecular vibrational energy redistribution (IVR) that is rapid compared to the rate of reaction/isomerization<sup>29–34</sup>. Such rapid IVR leads to a ‘loss of memory’ of particular initial conditions<sup>35</sup>. Standard computations based on features (usually critical points, such as minima and saddle points) of the potential energy surface (PES) then provide predictions for relative rates associated with competing reactive channels, temperature dependence of reaction rates and branching ratios, etc<sup>20–28,36</sup>. Nonstatistical effects can arise from a number of factors, which are certainly not mutually exclusive (see, for example, refs 37–43, also 44–53). The essential underlying reason is the ‘failure of ergodicity’, a property which is notoriously difficult either to predict or diagnose. Branching ratios and/or stereochemistries significantly different from statistical predictions can result from symmetry breaking induced by dynamics<sup>3</sup>.

The range of thermal organic reactions now believed to manifest some kind of nonstatistical behavior is extraordinarily diverse (see, for example, refs 3,7, and refs therein). A general characteristic shared by the systems for which the standard statistical theories fail is that the associated PES corresponds poorly if at all to the standard textbook picture of a 1D reaction coordinate passing over high barriers connecting deep wells (intermediates or reactants/products, cf. Fig. 1a)<sup>2,3,7</sup>. More specifically, the reaction coordinate (understood in the

broadest sense<sup>54,55</sup>) is inherently *multidimensional*, as are corresponding relevant phase space structures: there may exist extremely flat, plateau regions on the PES, with a number of exit channels characterised by low barriers<sup>2,3</sup>, or the PES may exhibit *bifurcations* of the reaction path<sup>56–60</sup> in the vicinity of so-called valley-ridge inflection (VRI) points<sup>9–11,16</sup> (see Fig. 1b). In the case of systems having dynamically relevant VRI points on/near the reaction path, outstanding fundamental questions remain concerning the effectiveness of approaches such as variational TST<sup>61–63</sup> or modified statistical theories<sup>64</sup> as opposed to full-scale trajectory simulations of the reaction dynamics<sup>65,66</sup>.

Other systems for which the standard 1D reaction coordinate picture is not valid include the growing class of so-called non-MEP (minimum energy path) reactions<sup>2,43,67–72</sup> and “roaming” mechanisms<sup>73–80</sup>; the dynamics of these reactions is not mediated by a single conventional transition state associated with an index 1 saddle.

The work just described highlights the basic importance of *momentum* for the outcome of a chemical reaction<sup>3,81</sup>; that is, a *phase space*<sup>82</sup> approach to reaction dynamics is needed<sup>83</sup>, as opposed to a view wedded solely to the topography of the PES<sup>36,84</sup>. For example, a symmetric PES with two symmetry-related reaction channels can give rise to asymmetric product distributions if nonsymmetric initial momentum distributions are created under experimental conditions<sup>3</sup>.

There have been significant recent theoretical and computational advances in the application of dynamical systems theory<sup>82,85–87</sup> to study reaction dynamics and phase space structure in multimode models of molecular systems, and to probe the dynamical origins of nonstatistical behavior<sup>83,88–99</sup> (see also refs 100–110). A phase space approach is essential to obtain a rigorous dynamical definition of the TS in multimode systems, this being the Normally Hyperbolic Invariant Manifold (NHIM)<sup>83</sup>. The NHIM generalizes the concept of the periodic orbit dividing surface (PODS)<sup>111–113</sup> to  $N \geq 3$  mode systems. A recent reappraisal of the *gap time* formalism for unimolecular rates<sup>98</sup> has led to novel diagnostics for nonstatistical behavior (‘nonexponential decay’) in isomerization processes, leading to a necessary condition for ergodicity.

In the present paper we study dynamics on a model potential energy surface (PES) exhibiting post-transition state bifurcation in the vicinity of a valley ridge inflection point (cf. Fig. 1b). A computed normal form (NF) is used to sample the dividing surface (DS) at fixed

total energy at the ‘incoming’ TS located at a point of high potential energy. (For previous discussion of sampling using normal forms, see ref. 99.) Bundles of trajectories so defined are then followed into the region of the PES where bifurcation of the reaction path occurs, and the subsequent dynamics studied. A key goal here is to obtain a dynamical understanding of the computed *branching ratio* for products reached after the VRI region is traversed. By changing parameters in the model potential, it is for example possible to alter the location but not the energy of one of the product minima, while keeping the energies and locations of other critical points unchanged. We find that apparently minor variations in the potential can lead to significant changes in the reaction dynamics.

The work described below leads to the following picture of the dynamical origin of the selectivity: for the model studied, the dynamics proceeds on at least 2 timescales. First, on short times, the bundle of trajectories ‘reflects’ off a hard wall that is opposite the high energy TS through which it enters the reaction zone. After this collision, a highly non-statistical and time-dependent population ratio of products is established, whose value depends on the direction in which trajectories are reflected by the (asymmetric) potential wall. These initial nonstatistical populations then relax on a somewhat longer timescale to yield the observed product ratio. During this phase of the reaction, there is the possibility of competition between IVR and other mechanisms for removing vibrational energy from active degrees of freedom (cf., for example, ref. 18). We explore one aspect of this phase of the dynamics by introducing dissipation into the model. Major conclusions are that, for this model at least, (i) the dynamics in the vicinity of the VRI point plays essentially no role in determining the product ratio, except in the highly dissipative regime, and (ii) the product ratio is a highly nonmonotonic function of the dissipation strength.

The structure of this paper is as follows: in Sec. II we introduce the model potential energy function to be studied. We compute the IRC path<sup>114</sup> connecting the TS to one or the other product minima, discuss the location of the VRI point<sup>56-58</sup>, and compute Newton trajectories<sup>115,116</sup> and gradient extremals<sup>117,118</sup>. In Section III we formulate the equations of motion used to calculate reaction dynamics on our model surface with and without dissipation, and discuss the specification of initial conditions on the DS. Results are presented in Sec. IV: dynamics of trajectory bundles and product ratios at fixed energies with and without dissipation, and fractional product yields as a function of dissipation parameter. Sec. V con-

cludes. Details on the computations required to locate the VRI point are given in Appendix A.

## II. POTENTIAL ENERGY SURFACE

In this work we investigate, using classical trajectories, reaction dynamics on a model potential surface exhibiting a valley ridge inflection (VRI) point (cf. Figure 1b).

The potential studied exhibits an index 1 saddle (‘transition state’, TS) at high energy. Trajectories are initiated on the DS associated with this (upper, high energy) saddle, and can form either of two products. (There is also the possibility that trajectories can exit via the high energy transition state; on sufficiently long timescales, all trajectories [excluding a set of measure zero] will escape through this ‘hole’ in the potential, provided that no energy dissipation is present.) Downhill in energy from the upper saddle point there is another index 1 saddle point, which forms a ‘ridge’, which is a conventional transition state for the isomerization reaction that interconverts the two products. Between the two saddle points there is therefore a VRI point<sup>56–58</sup>. Because the general form of the potential energy surface studied here is not fully symmetric with respect to the coordinate transformation  $y \rightarrow -y$  (see below), the intrinsic reaction path<sup>114</sup> does not in fact bifurcate, so that the location of the VRI point merely indicates the *region* of the PES where, in a naive conventional picture, trajectories ‘decide’ which product well to enter (see below). Most trajectories initiated on the upper DS do however pass through the neighborhood of the VRI point.

In addition to the trajectory studies reported in the following Section, we also present here results on the computation of various theoretical constructs associated with the concept of ‘reaction path’ for our model surface<sup>56–58,114–118</sup>. These are the IRC<sup>114</sup>, VRI points<sup>56–58</sup>, Newton trajectories<sup>115,116</sup> and gradient extremal paths<sup>117,118</sup>. It is worthwhile emphasizing that the various specific potential functions studied here do in fact have VRI points, despite not being fully symmetric. Our results provide a numerical demonstration that the mathematical conditions for the existence of a VRI (see below) can readily be satisfied in the absence of symmetry.

## A. Model potential

The system studied has 2 degrees of freedom (DoF), with associated coordinates  $(x, y)$ . The functional form is a modified version of a model potential previously introduced by Carpenter (see ref. 2):

$$V(x, y) = c_0 \left( \frac{1}{3}x^3 - \frac{1}{2}\alpha x^2 \right) + \omega^2 y^2 \frac{1}{2} (1 - \beta x) + c_1 y^4 x + c_2 x^2 y^2 + c_3 y x^2 + c_4 x y^2 + c_5 x y + c_6 x y^3. \quad (2.1)$$

We fix parameter values  $\alpha = 2$ ,  $\beta = 2$ ,  $c_0 = 3$ ,  $\omega = \sqrt{3}$ . The values of the remaining 6 parameters  $c_k$ ,  $k = 1, \dots, 6$  are then determined by specifying the locations and energies of the minima of the upper and lower product wells (6 parameters in all, obtained by solving a set of linear equations).

The upper index-1 saddle point is located at the origin  $(0, 0)$  with energy  $V_0 = 0$ . The coordinates of the lower product well ( $y < 0$ ) are fixed at  $(x, y) = (2.4, -1.2)$ , minimum energy  $v = -7.5$ . For the upper product well ( $y > 0$ ) we take coordinates  $(x, y) = (x^*, 1.2)$ , minimum energy  $v = -6$ . We consider 3 cases:  $x^* = 2.00$ ,  $x^* = 2.05$ ,  $x^* = 2.10$ . Values of the coefficients  $c_k$  for the 3 different cases are given in Table I.

## B. Reaction paths, bifurcations and valley ridge inflections

Figure 2 shows contour plots of the potentials corresponding to values  $x^* = 2.00$  and  $x^* = 2.10$ , respectively. Also shown are the corresponding IRC paths connecting the upper TS with one of the 2 product minima. These paths are computed in the standard way<sup>114</sup> as solutions of the differential equation

$$\frac{d\mathbf{r}}{ds} = -\nabla V \quad (2.2)$$

where  $\mathbf{r} = (x, y)$  and  $s$  parametrizes progress along the IRC. Since the mass  $m = 1$  for our model problem, there is no distinction between mass-weighted and unweighted coordinates.

For  $x^* = 2.00$  the IRC reaction path from the upper TS terminates at the upper minimum ( $y > 0$ ), while that for  $x^* = 2.10$  terminates at the lower minimum ( $y < 0$ ). (The  $x^* = 2.05$  potential [not shown in Figure 2] is also nonsymmetric; the IRC terminates at the upper minimum in this case.) Table II lists coordinates and energies of the critical points (index-1 saddles and minima) of potential eq. (2.1), computed for  $x^*$  values 2.00, 2.05 and 2.10

Additional quantities of interest are included in the contour plots of Fig. 2. The Hessian  $\mathcal{H}$  is the matrix of second derivatives

$$\mathcal{H} = \begin{bmatrix} V_{xx} & V_{xy} \\ V_{yx} & V_{yy} \end{bmatrix} \quad (2.3)$$

where subscripts indicate partial differentiation. (The mass tensor/kinetic energy is by definition trivial for our model, as we take  $m_x = m_y = 1$ . When defining the Hessian it is therefore not necessary to consider covariant derivatives of the potential, as would be required for the general case of a Hamiltonian having coordinate dependent kinetic energy<sup>119</sup>.) At a VRI point<sup>56-58</sup> (i) the Hessian matrix has a zero eigenvalue and (ii) the gradient vector  $\mathbf{g} = \nabla V$  is perpendicular to the corresponding eigenvector. As discussed in Appendix A, VRI points are found at the intersections of zero contours of the quantities  $\mathbf{g} \cdot \text{adj}[\mathcal{H}] \cdot \mathbf{g}$  and  $\det[\mathcal{H}]$ , where the adjugate matrix  $\text{adj}[\mathcal{H}] = \det[\mathcal{H}]\mathcal{H}^{-1}$ .

For each value  $x^* = 2.0$  and  $x^* = 2.1$ , we show in Fig. 2 the zero contours of the determinant of the Hessian matrix  $\mathcal{H}$  (red) and of the quantity  $\mathbf{g} \cdot \text{adj}[\mathcal{H}] \cdot \mathbf{g}$  (green). Each plot exhibits a single VRI point at the intersection of the 2 contour lines, close to *but not actually on* the IRC path. The locations of the VRI points for  $x^*$  values 2.00, 2.05 and 2.10 are listed in Table II.

In Figure 3a we plot a set of Newton trajectories<sup>115,116</sup> for the case  $x^* = 2.05$ . At every point along a Newton trajectory, the gradient vector  $\mathbf{g}$  points in a fixed direction specified by a search vector  $\mathbf{r}$ <sup>116</sup>. Figure 3a shows Newton trajectories computed for unit search vectors  $\mathbf{r} = \{\cos[\theta], \sin[\theta]\}$ , for a number of angles  $\theta$  sampled uniformly in the interval  $0 \leq \theta \leq \pi$ . (In fact, the “trajectories” are computed as the zero contours of the function  $f = \mathbf{r}_\perp \cdot \mathbf{g}$ , where  $\mathbf{r}_\perp = \{-\sin[\theta], \cos[\theta]\}$  is a unit vector perpendicular to  $\mathbf{r}$ .)

Our results illustrate the fact that (complete) Newton trajectories connect all stationary points on the potential, and that bifurcations of Newton trajectories occur at VRI points<sup>116</sup>. These properties make Newton trajectories very useful for exploration of PES features. Nevertheless, comparison with dynamical trajectories (see below) shows that, at least for the potential studied here, Newton trajectories provide little insight into the actual reactive dynamics.

In Figure 3b we plot gradient extremal paths<sup>117,118</sup> for the case  $x^* = 2.05$ . At gradient



extremal points, the gradient vector  $\mathbf{g}$  is an eigenvector of the Hessian

$$\mathcal{H}\mathbf{g} \propto \mathbf{g}. \tag{2.4}$$

The gradient extremal paths plotted are actually obtained by computing the zero contours of the quantity<sup>118,120</sup>

$$\Gamma = V_{xy}(V_x^2 - V_y^2) + (V_{yy} - V_{xx})V_xV_y. \tag{2.5}$$

It can be seen that, in contrast to the IRC path, the gradient extremal path connects the upper and lower index 1 saddles, even for a non-symmetric potential. The two index 1 saddle points are also connected by singular Newton trajectories (Fig. 3a). However, it is also seen that gradient extremal paths can exhibit loops and turning points, limiting their utility as models for reaction paths.

### III. TRAJECTORY CALCULATIONS: HAMILTONIAN, DISSIPATION AND INITIAL CONDITIONS

We study reaction dynamics using a Hamiltonian based on the 2 DoF potential eq. (2.1). We therefore effectively consider the dynamics on a timescale short enough so that transfer of energy to or from other degrees of freedom (intramolecular vibrational modes, solvent bath modes) is negligible. In addition, we do however (crudely) model the effect of additional degrees of freedom by introducing dissipation into our model. Explicit inclusion of additional degrees of freedom is left for future investigations.

#### A. Equations of motion

The Hamiltonian has the form:

$$H(x, y, p_x, p_y) = \frac{p_x^2}{2} + \frac{p_y^2}{2} + V(x, y), \tag{3.1}$$

with potential  $V(x, y)$  given by eq. (2.1) and Hamilton's equations of motion:

$$\dot{x} = p_x, \tag{3.2a}$$

$$\dot{y} = p_y, \tag{3.2b}$$

$$\dot{p}_x = -\frac{\partial V}{\partial x}(x, y), \tag{3.2c}$$

$$\dot{p}_y = -\frac{\partial V}{\partial y}(x, y). \tag{3.2d}$$

The effects of dissipation are modelled by adding a simple damping term to equations of motion (3.2) as follows:

$$\dot{x} = p_x, \tag{3.3a}$$

$$\dot{y} = p_y, \tag{3.3b}$$

$$\dot{p}_x = -\frac{\partial V}{\partial x}(x, y) - \gamma_x p_x, \tag{3.3c}$$

$$\dot{p}_y = -\frac{\partial V}{\partial y}(x, y) - \gamma_y p_y. \tag{3.3d}$$

for some  $\gamma_x, \gamma_y > 0$ , so that the kinetic energy monotonically decreases along the trajectory. We set  $\gamma_x = \gamma_y \equiv \gamma$  and study the effects of dissipation for a range of  $\gamma$  values  $0 \leq \gamma \leq 1$ . In the present calculations, random thermal fluctuations (e.g., Langevin dynamics<sup>121</sup>) are not considered.

## B. Initial conditions

Trajectories are initiated on the phase space DS associated with the transition state located at the high energy saddle point. A normal form<sup>83</sup> of degree 10 is computed, and the dividing surface sampled using a grid in phase space at a specified energy<sup>99</sup>. We integrate trajectories and compute product fractional yield (equivalently, branching ratio) as a function of time.

In order to decide whether a trajectory is in the upper or lower product well, we define a plane in phase space tangent to the dividing surface separating the two products; this surface is computed from a normal form constructed at the lower (ridge) saddle point. The sign of the standard inner product of the displacement vector of a phase point from the lower saddle with a vector normal to the tangent plane then determines the well to which the point is assigned. Trajectories are stopped if they re-cross the upper saddle DS but few such

cases were observed (for the integration times used), and none for any nonzero values of the dissipation factor  $\gamma$  (see below).

The effects of dissipation are modelled by integrating eq. (3.3) for a range of values of the dissipation parameter  $\gamma$ . Initial conditions for trajectory calculations incorporating dissipation are sampled on the DS in the usual way using Hamiltonian (3.2) for a fixed value of the initial energy.

## IV. RESULTS

### A. Reaction dynamics without dissipation

Figure 4 shows the behavior of bundles of 64 trajectories initiated on the DS at the upper TS, with energy  $E = 0.1$  above the saddle energy. (Recall that the energy of the upper saddle is  $E = 0$ , the energy of the lower saddle is  $E \sim -4.0$ , while the product minima are at energies  $E = -6.0$  and  $E = -7.5$ , respectively.) We show results for the 2 cases  $x^* = 2.0$  and  $x^* = 2.1$ , respectively. Trajectories are integrated for  $t_{\max} = 4$  time units, a time comparable to the natural period for motion in either well.

Figure 5 shows corresponding trajectory bundles at  $E = 0.01$  above the saddle energy. These lower energy trajectories are integrated for longer times, up to  $t_{\max} = 8$ .

All trajectories initially collide with the hard wall of the potential that is directly ‘downhill’ from the upper TS. This collision is followed by a number of more or less ‘coherent’ oscillations of the trajectory bundle between product wells, with concurrent dephasing. The well occupancies (product yields) shown in Figs 4 and 5 clearly demonstrate the coherent short-time behavior of the trajectory bundles, and the dramatic effect on well occupancies brought about by apparently minor changes in potential topography.

Changing the location of the upper minimum, specifically the  $x$ -coordinate  $x^*$ , also changes the curvature of the potential in the vicinity of the ‘hard wall’ encountered by trajectories after they have rolled downhill from the upper TS. This change in curvature in turn affects the direction in which the trajectory bundle is predominantly ‘reflected’ by the hard wall, as can be seen from the time-dependent product yields (fractions) shown in Figures 4 and 5

Figure 6 shows well occupancies for the 2 cases  $x^* = 2.0$  and  $x^* = 2.1$  for  $0 \leq t \leq t_{\max} = 100$ . Even at  $t = t_{\max}$ , the ratio of well occupancies apparently has not converged to an

asymptotic (steady state) value. That is, nontrivial isomerization dynamics is still occurring. These fluctuations may however reflect the finite size of the trajectory ensemble used in our calculations. Figure 6 also shows that the cumulative fraction of trajectories that escape (recross the upper DS) is small but non-negligible for both cases.

We next consider the addition of dissipative damping, which ensures that the branching ratio becomes well defined at relatively short times.

### B. Reaction dynamics with dissipation

Figure 7 shows 2 trajectory bundles at  $E = 0.01$  with the relatively large dissipation factor  $\gamma = 0.5$  (64 trajectories per bundle). The trajectories drop into one of the wells within approximately 4 time units, and, as anticipated for the highly dissipative case, the predominant product obtained is determined by the IRC path from the upper TS. Note that the product ratio inverts between the two cases, which differ *only* in the value of  $x^*$ .

Figure 8 shows the behavior of trajectory bundles at  $E = 0.01$  for a smaller dissipation factor  $\gamma = 0.25$  together with corresponding well occupancies, for  $0 \leq t \leq t_{\max} = 5$ . For  $x^* = 2.1$ , the product ratio at long times is now reversed with respect to the value for  $\gamma = 0.5$ ; for the lower dissipation parameter, trajectories are able to cross the ridge separating products one more time (on average) before losing energy and becoming trapped in one or the other well.

These results suggest the interesting possibility that the branching ratios might exhibit a *non-monotonic* dependence on dissipation parameter. This question is explored below.

### C. Product ratios as a function of dissipation parameter

We now examine systematically the behavior of fractional product yields as a function of the dissipation parameter. The branching ratio is given in terms of the fraction of trajectories which are in either of the two wells after the system has settled down and trajectories no longer have sufficient energy to cross the ridge. As the dissipation factor  $\gamma$  becomes smaller, it is necessary to follow trajectory ensembles for longer and longer times to determine asymptotic product ratios.

Note that, although our trajectory calculations examine the fate of ensembles of trajectories initiated on the DS at a fixed time, the branching ratios we compute are nevertheless equally applicable to the situation in which a steady stream of reactants passes over the upper TS.

We compute fractional product yields for a range of dissipation parameter  $0.01 \leq \gamma \leq 1$ . We have checked that our results are converged both with respect to the trajectory run time  $t_{\max}$  and the size of the ensemble.

Figure 9 shows the fraction of trajectories in the lower well as a function of dissipation parameter  $\gamma$  for  $x^* = 2.0$  (Fig. 9a),  $x^* = 2.05$  (Fig. 9b) and  $x^* = 2.1$  (Fig. 9c) for  $E = 0.01$ . For each case, the fraction of given product is a highly structured non-monotonic function of the dissipation parameter  $\gamma$ . It is moreover striking that minor variations in the value of  $x^*$  lead to noticeably different dependence of yield on  $\gamma$ . Figure 9d shows the fractional yield for  $x^* = 2.05$  at the higher energy  $E = 0.1$  above threshold; the behavior is very similar to that seen at the lower energy  $E = 0.01$ .

The nontrivial dependence of branching ratios on  $\gamma$  has its origin in the interplay between the almost coherent ridge crossing dynamics of the trajectory bundle and the dissipative loss of kinetic energy, leading to trapping of trajectories in one or the other well. The dissipation rate sets the timescale on which trajectories settle into their final associated product wells.

This interpretation of the branching ratio results is confirmed by examining the dynamics of trajectory bundles in more detail. For example, Figure 10 shows time-dependent fractional yields and trajectory segments ( $t_1 \leq t \leq t_2$ ) for the intermediate case  $x^* = 2.05$  at initial energy  $E = 0.01$  for 2 dissipation parameters,  $\gamma = 0.13$  and  $\gamma = 0.1$ , respectively. Ensemble trajectory segments for the ensemble are shown with  $t_1 = 8.5$ ,  $t_2 = 9.0$ . With these values of  $t_1$  and  $t_2$  it can be seen that for the larger dissipation parameter the final product well is already determined for all trajectories in the ensemble, while reducing the dissipation parameter slightly allows some additional ridge crossing, changing the branching ratio significantly.

The coherent crossing of the central ridge causes trajectories to sample one product well and then the other in an oscillatory fashion. Similar phenomena have been seen in trajectory simulations of a number of unimolecular reactions of polyatomic systems<sup>17,122</sup>, suggesting that the present behavior might persist on at least some higher dimensional potential energy surfaces. This question is under active investigation.

## V. SUMMARY AND CONCLUSIONS

We have studied reaction dynamics on a model potential energy surface exhibiting post-transition state bifurcation in the vicinity of a valley ridge inflection point. Bundles of trajectories initiated on the dividing surface associated with a high energy TS are followed into the region of the PES where bifurcation of the reaction path occurs, and the subsequent dynamics studied. We have computed fractional yields for products reached after the VRI region is traversed, both with and without dissipation. It is found that apparently minor variations in the potential lead to significant changes in the reaction dynamics. Moreover, the branching ratio depends in a complicated and highly non-monotonic fashion on the dissipation parameter.

For the model considered here, the dynamics proceeds on at least two timescales. First, on short times, the bundle of trajectories ‘reflects’ off a hard wall that is opposite the high energy TS through which it enters the reaction zone. After this collision, a highly non-statistical and time-dependent population ratio of products is established, whose value depends on the direction in which trajectories are reflected by the (asymmetric) potential wall. These initial nonstatistical populations then relax on a somewhat longer timescale to yield the observed product ratio. During this phase of the reaction, there is the possibility of competition between IVR and other mechanisms for removing vibrational energy from active degrees of freedom. Introducing dissipation into the model sets the timescale on which the branching ratio is determined.

One would expect that for real chemical systems, reactions in condensed phases would be characterized by higher dissipation rates<sup>123</sup> and that some control of collision-induced dissipation might be attainable through the use of supercritical fluids at variable pressure<sup>124</sup>. However, to our knowledge, such techniques have not yet been applied to any reaction for which the existence of a chemically significant VRI has been established.

Overall, we find that dynamics in the vicinity of the VRI point on the potential play essentially no role in determining the product ratio, except in the highly dissipative regime. Extension of these investigations to more realistic theoretical models of reactions involving VRI points (see, for example, refs 67,125–128) is a topic of current research.

## Acknowledgments

We are grateful to Dr. Zeb Kramer for his penetrating comments on the manuscript.

PC and SW acknowledge the support of the Office of Naval Research (Grant No. N00014-01-1-0769). PC, BKC and SW acknowledge the support of the UK Engineering and Physical Sciences Research Council (Grant No. EP/K000489/1). The work of GSE is supported by the US National Science Foundation under Grant No. CHE-1223754.

## Appendix A: Location of VRI points

The Hessian matrix  $\mathcal{H}$  is a real symmetric matrix, and has 2 real eigenvalues and associated orthonormal eigenvectors. Let the eigenvalues and eigenvectors of  $\mathcal{H}$  be denoted  $\lambda_\alpha$  and  $\mathbf{v}_\alpha$ , respectively,  $\alpha = 1, 2$ . The potential gradient vector  $\mathbf{g} = \nabla V$  is then decomposed as follows:

$$\mathbf{g} = \sum_{\alpha} \mathbf{v}_\alpha c_\alpha. \quad (\text{A1})$$

Defining the *adjugate* matrix  $\text{adj}[\mathcal{H}] \equiv \det[\mathcal{H}] \mathcal{H}^{-1}$ , we have

$$\mathbf{g} \cdot \text{adj}[\mathcal{H}] \cdot \mathbf{g} = \sum_{\alpha} \lambda_{\alpha'} c_\alpha^2 \quad (\text{A2})$$

where  $\alpha' = 2$  if  $\alpha = 1$ , and vice versa. The quantity  $\mathbf{g} \cdot \text{adj}[\mathcal{H}] \cdot \mathbf{g}$  is the second-order variation in the potential along a vector perpendicular to  $\mathbf{g}$  (having the same length). The condition

$$\mathbf{g} \cdot \text{adj}[\mathcal{H}] \cdot \mathbf{g} = 0 \quad (\text{A3})$$

therefore implies

$$c_1^2 \lambda_2 = -c_2^2 \lambda_1. \quad (\text{A4})$$

At the VRI point, there is an eigenvector perpendicular to the gradient vector  $\mathbf{g}$  with associated eigenvalue zero. Therefore, at the VRI point, both condition (A3) and the condition

$$\det[\mathcal{H}] = \lambda_1 \lambda_2 = 0 \quad (\text{A5})$$

must hold. We therefore find the VRI point(s) numerically by locating the intersection(s) of the zero contours of  $\det[\mathcal{H}]$  and  $\mathbf{g} \cdot \text{adj}[\mathcal{H}] \cdot \mathbf{g}$ .

---

\* CarpenterB1@cardiff.ac.uk

† gse1@cornell.edu

‡ stephen.wiggins@mac.com

- <sup>1</sup> B. K. Carpenter, *Acc. Chem. Res.* **25**, 520 (1992).
- <sup>2</sup> B. K. Carpenter, in *Reactive Intermediate Chemistry*, edited by R. A. Moss and M. S. Platz and M. Jones Jr. (Wiley, New York, 2004), pp. 925–960.
- <sup>3</sup> B. K. Carpenter, *Ann. Rev. Phys. Chem.* **56**, 57 (2005).
- <sup>4</sup> D. M. Bachrach, *Computational Organic Chemistry* (Wiley Interscience, New York, 2007).
- <sup>5</sup> D. Birney, *Current Organic Chemistry* **14**, 1658 (2010).
- <sup>6</sup> H. Yamataka, *Adv. Phys. Org. Chem.* **44**, 173 (2010).
- <sup>7</sup> J. Rehbein and B. Carpenter, *PCCP* **13**, 20906 (2011).
- <sup>8</sup> B. Ussing, C. Hang, and D. Singleton, *JACS* **128**, 7594 (2006).
- <sup>9</sup> J. Thomas, J. Waas, M. Harmata, and D. Singleton, *JACS* **130**, 14544 (2008).
- <sup>10</sup> D. H. Ess, S. E. Wheeler, R. G. Iafe, L. Xu, N. Celebi-Olcum, and K. N. Houk, *Angew. Chemie* **47**, 7592 (2008).
- <sup>11</sup> Z. Wang, J. S. H. Jennifer, and D. A. Singleton, *Angew. Chemie Intl. Ed.* **48**, 9156 (2009).
- <sup>12</sup> Y. Oyola and D. Singleton, *JACS* **131**, 3130 (2009).
- <sup>13</sup> Y. H. Young and D. J. Tantillo, *Nature Chem.* **1**, 384 (2009).
- <sup>14</sup> D. Glowacki, S. M. Stephen, and M. Pilling, *JACS* **131**, 13896 (2009).
- <sup>15</sup> T. Katori, S. Itoh, M. Sato, and H. Yamataka, *JACS* **132**, 3413 (2010).
- <sup>16</sup> M. Siebert, J. Zhang, S. Addepalli, D. Tantillo, and W. Hase, *JACS* **133**, 8335 (2011).
- <sup>17</sup> L. Goldman, D. Glowacki, and B. Carpenter, *JACS* **133**, 5312 (2011).
- <sup>18</sup> L. Quijano and D. Singleton, *JACS* **133**, 13824 (2011).
- <sup>19</sup> Y. Yamamoto, H. Hasegawa, and H. Yamataka, *J. Org. Chem.* **76**, 4652 (2011).
- <sup>20</sup> E. P. Wigner, *Trans. Faraday Soc.* **34**, 29 (1938).
- <sup>21</sup> D. L. Bunker, *Theory of Elementary Gas Reaction Rates* (Pergamon, Oxford, 1966).
- <sup>22</sup> P. J. Robinson and K. A. Holbrook, *Unimolecular Reactions* (Wiley, New York, 1972).
- <sup>23</sup> W. Forst, *Theory of Unimolecular Reactions* (Academic, New York, 1973).
- <sup>24</sup> T. Baer and W. L. Hase, *Unimolecular Reaction Dynamics* (Oxford University Press, New York, 1996).
- <sup>25</sup> D. G. Truhlar, B. C. Garrett, and S. J. Klippenstein, *J. Phys. Chem.* **100**, 12771 (1996).



- <sup>26</sup> W. Forst, *Unimolecular Reactions* (Cambridge University Press, Cambridge, 2003).
- <sup>27</sup> N. E. Henriksen and F. Y. Hansen, *Theories of Molecular Reaction Dynamics: The Microscopic Foundation of Chemical Kinetics* (Oxford University Press, New York, 2008).
- <sup>28</sup> B. K. Carpenter, *Determination of Organic Reaction Mechanisms* (Wiley, New York, 1984).
- <sup>29</sup> M. Tabor, *Adv. Chem. Phys.* **XLVI**, 73 (1981).
- <sup>30</sup> S. A. Rice, *Adv. Chem. Phys.* **XLVII**, 117 (1981).
- <sup>31</sup> P. Brumer, *Adv. Chem. Phys.* **XLVII**, 201 (1981).
- <sup>32</sup> D. W. Noid, M. L. Koszykowski, and R. A. Marcus, *Ann. Rev. Phys. Chem.* **32**, 267 (1981).
- <sup>33</sup> P. Brumer and M. Shapiro, *Adv. Chem. Phys.* **70**, 365 (1988).
- <sup>34</sup> T. A. Uzer and W. H. Miller, *Phys. Rep.* **199**, 73 (1991).
- <sup>35</sup> O. Brass and C. Schlier, *J. Chem. Soc. Farad. Trans.* **89**, 1533 (1993).
- <sup>36</sup> D. J. Wales, *Energy Landscapes* (Cambridge University Press, Cambridge, 2003).
- <sup>37</sup> D. L. Bunker, *J. Chem. Phys.* **37**, 393 (1962).
- <sup>38</sup> D. L. Bunker, *J. Chem. Phys.* **40**, 1946 (1964).
- <sup>39</sup> W. L. Hase, in *Modern Theoretical Chemistry*, edited by W. H. Miller (Plenum, New York, 1976), vol. 2, pp. 121–170.
- <sup>40</sup> W. L. Hase, *Acc. Chem. Res.* **31**, 659 (1998).
- <sup>41</sup> S. Y. Grebenshchikov, R. Schinke, and W. L. Hase, in *Unimolecular Kinetics: Part 1. The Reaction Step*, edited by N. J. B. Greene (Elsevier, New York, 2003), vol. 39 of *Comprehensive Chemical Kinetics*, pp. 105–242.
- <sup>42</sup> A. Bach, J. M. Hostettler, and P. Chen, *J. Chem. Phys.* **125**, Art. No. 024304 (2006).
- <sup>43</sup> U. Lourderaj and W. L. Hase, *J. Phys. Chem. A* **113**, 2236 (2009).
- <sup>44</sup> S. A. Schofield and P. G. Wolynes, *Chem. Phys. Lett.* **217**, 497 (1994).
- <sup>45</sup> S. A. Schofield, P. G. Wolynes, and R. E. Wyatt, *Phys. Rev. Lett.* **74**, 3720 (1995).
- <sup>46</sup> S. A. Schofield and P. G. Wolynes, *J. Phys. Chem.* **99**, 2753 (1995).
- <sup>47</sup> D. M. Leitner and P. G. Wolynes, *Phys. Rev. Lett.* **76**, 216 (1996).
- <sup>48</sup> D. M. Leitner and P. G. Wolynes, *Chem. Phys. Lett.* **280**, 411 (1997).
- <sup>49</sup> W. L. Hase, *Science* **266**, 998 (1994).
- <sup>50</sup> M. Gruebele and P. G. Wolynes, *Acc. Chem. Res.* **37**, 261 (2004).
- <sup>51</sup> D. M. Leitner and P. G. Wolynes, *Chem. Phys.* **329**, 163 (2006).

- <sup>52</sup> D. M. Leitner and M. Gruebele, *Mol. Phys.* **106**, 433 (2008).
- <sup>53</sup> D. M. Leitner, Y. Matsunaga, C.-B. Li, T. Komatsuzaki, A. Shojiguchi, and M. Toda, *Adv. Chem. Phys.* **145**, 83 (2011).
- <sup>54</sup> D. Heidrich, ed., *The Reaction Path in Chemistry: Current Approaches and Perspectives* (Springer, New York, 1995).
- <sup>55</sup> E. Kraka, *Wiley Interdisciplinary Reviews: Computational Molecular Science* **1**, 531 (2011).
- <sup>56</sup> P. Valtazanos and K. Reudenberg, *Theo. Chim. Acta* **69**, 281 (1986).
- <sup>57</sup> W. Quapp, M. Hirsch, and D. Heidrich, *Theo. Chem. Acc.* **100**, 285 (1998).
- <sup>58</sup> W. Quapp, *J. Mol. Struct.* **695**, 95 (2004).
- <sup>59</sup> B. Lasorne, G. Dive, and M. Desouter-Lecomte, *J. Chem. Phys.* **122**, 184304 (2005).
- <sup>60</sup> D. Sugny, C. Kontz, M. Ndong, Y. Justum, G. Dive, and M. Desouter-Lecomte, *Phys. Rev. A* **74**, 043419 (2006).
- <sup>61</sup> J. C. Keck, *Adv. Chem. Phys.* **XIII**, 85 (1967).
- <sup>62</sup> W. L. Hase, *Acc. Chem. Res.* **16**, 258 (1983).
- <sup>63</sup> D. G. Truhlar and B. C. Garrett, *Ann. Rev. Phys. Chem.* **35**, 159 (1984).
- <sup>64</sup> J. Zheng, E. Papajak, and D. Truhlar, *JACS* **131**, 15754 (2009).
- <sup>65</sup> A. Gonzalez-Lafont, M. Moreno, and J. Lluch, *JACS* **126**, 13089 (2004).
- <sup>66</sup> J. Ramirez-Anguita, R. Gelabert, A. Gonzalez-Lafont, M. Moreno, and J. M. Lluch, *Theo. Chem. Acc.* **128**, 569 (2011).
- <sup>67</sup> D. J. Mann and W. L. Hase, *JACS* **124**, 3208 (2002).
- <sup>68</sup> L. P. Sun, K. Y. Song, and W. L. Hase, *Science* **296**, 875 (2002).
- <sup>69</sup> S. L. Debbert, B. K. Carpenter, D. A. Hrovat, and W. T. Borden, *J. Am. Chem. Soc.* **124**, 7896 (2002).
- <sup>70</sup> S. C. Ammal, H. Yamataka, M. Aida, and M. Dupuis, *Science* **299**, 1555 (2003).
- <sup>71</sup> J. G. Lopez, G. Vayner, U. Lourderaj, S. V. Addepalli, S. Kato, W. A. Dejong, T. L. Windus, and W. L. Hase, *J. Am. Chem. Soc.* **129**, 9976 (2007).
- <sup>72</sup> U. Lourderaj, K. Park, and W. L. Hase, *Int. Rev. Phys. Chem.* **27**, 361 (2008).
- <sup>73</sup> D. Townsend, S. A. Lahankar, S. K. Lee, S. D. Chambreau, A. G. Suits, X. Zhang, J. Rheinecker, L. B. Harding, and J. M. Bowman, *Science* **306**, 1158 (2004).
- <sup>74</sup> J. M. Bowman, *PNAS* **103**, 16061 (2006).

- <sup>75</sup> B. C. Shepler, B. J. Braams, and J. M. Bowman, *J. Phys. Chem. A* **111**, 8282 (2007).
- <sup>76</sup> B. C. Shepler, B. J. Braams, and J. M. Bowman, *J. Phys. Chem. A* **112**, 9344 (2008).
- <sup>77</sup> A. G. Suits, *Acc. Chem. Res.* **41**, 873 (2008).
- <sup>78</sup> B. R. Heazlewood, M. J. T. Jordan, S. H. Kable, T. M. Selby, D. L. Osborn, B. C. Shepler, B. J. Braams, and J. M. Bowman, *PNAS* **105**, 12719 (2008).
- <sup>79</sup> J. Bowman and A. Suits, *Physics Today* **64**(11), 33 (2011).
- <sup>80</sup> J. Bowman and B. Shepler, *Ann. Rev. Phys. Chem.* **62**, 531 (2011).
- <sup>81</sup> B. Carpenter, *Angew. Chemie (Intl Ed.)* **37**, 3341 (1998).
- <sup>82</sup> R. S. MacKay and J. D. Meiss, *Hamiltonian Dynamical Systems: A reprint selection* (Taylor and Francis, London, 1987).
- <sup>83</sup> H. Waalkens, R. Schubert, and S. Wiggins, *Nonlinearity* **21**, R1 (2008).
- <sup>84</sup> P. G. Mezey, *Potential Energy Hypersurfaces* (Elsevier, Amsterdam, 1987).
- <sup>85</sup> A. J. Lichtenberg and M. A. Lieberman, *Regular and Chaotic Dynamics* (Springer Verlag, New York, 1992), 2nd ed.
- <sup>86</sup> S. Wiggins, *Chaotic transport in dynamical systems* (Springer-Verlag, 1992).
- <sup>87</sup> V. I. Arnold, V. V. Kozlov, and A. I. Neishtadt, *Mathematical Aspects of Classical and Celestial Mechanics* (Springer, New York, 2006).
- <sup>88</sup> S. Wiggins, *Physica D* **44**, 471 (1990).
- <sup>89</sup> S. Wiggins, L. Wiesenfeld, C. Jaffe, and T. Uzer, *Phys. Rev. Lett.* **86**(24), 5478 (2001).
- <sup>90</sup> T. Uzer, C. Jaffe, J. Palacian, P. Yanguas, and S. Wiggins, *Nonlinearity* **15**, 957 (2002).
- <sup>91</sup> H. Waalkens, A. Burbanks, and S. Wiggins, *J. Phys. A* **37**, L257 (2004).
- <sup>92</sup> H. Waalkens and S. Wiggins, *J. Phys. A* **37**, L435 (2004).
- <sup>93</sup> H. Waalkens, A. Burbanks, and S. Wiggins, *J. Chem. Phys.* **121**(13), 6207 (2004).
- <sup>94</sup> H. Waalkens, A. Burbanks, and S. Wiggins, *Physical Review Letters* **95**, 084301 (2005).
- <sup>95</sup> H. Waalkens, A. Burbanks, and S. Wiggins, *J. Phys. A* **38**, L759 (2005).
- <sup>96</sup> R. Schubert, H. Waalkens, and S. Wiggins, *Phys. Rev. Lett.* **96**, 218302 (2006).
- <sup>97</sup> G. S. Ezra and S. Wiggins, *J. Phys. A (Fast track communication)* **42**, 042001 (2009).
- <sup>98</sup> G. S. Ezra, H. Waalkens, and S. Wiggins, *J. Chem. Phys.* **130**, 164118 (2009).
- <sup>99</sup> P. Collins, G. S. Ezra, and S. Wiggins, *J. Chem. Phys.* **134**, 244105 (2011).
- <sup>100</sup> T. Komatsuzaki and R. S. Berry, *J. Mol. Struct. THEOCHEM* **506**, 55 (2000).

- <sup>101</sup> T. Komatsuzaki and R. S. Berry, *Adv. Chem. Phys.* **123**, 79 (2002).
- <sup>102</sup> M. Toda, *Adv. Chem. Phys.* **123**, 153 (2002).
- <sup>103</sup> T. Komatsuzaki, K. Hoshino, and Y. Matsunaga, *Adv. Chem. Phys.* **130 B**, 257 (2005).
- <sup>104</sup> L. Wiesenfeld, A. Faure, and T. Johann, *J. Phys. B* **36**, 1319 (2003).
- <sup>105</sup> L. Wiesenfeld, *J. Phys. A* **37**, L143 (2004).
- <sup>106</sup> L. Wiesenfeld, *Few Body Syst.* **34**, 163 (2004).
- <sup>107</sup> M. Toda, *Adv. Chem. Phys.* **130 A**, 337 (2005).
- <sup>108</sup> F. Gabern, W. S. Koon, J. E. Marsden, and S. D. Ross, *Physica D* **211**, 391 (2005).
- <sup>109</sup> F. Gabern, W. S. Koon, J. E. Marsden, and S. D. Ross, *Few-Body Systems* **38**, 167 (2006).
- <sup>110</sup> A. Shojiguchi, C. B. Li, T. Komatsuzaki, and M. Toda, *Comm. Nonlinear Sci. Numerical Simulation* **13**, 857 (2008).
- <sup>111</sup> E. Pollak and P. Pechukas, *J. Chem. Phys.* **69**, 1218 (1978).
- <sup>112</sup> P. Pechukas, *Ann. Rev. Phys. Chem.* **32**, 159 (1981).
- <sup>113</sup> P. Pechukas, *Ber. Buns. Ges.* **86**, 372 (1982).
- <sup>114</sup> K. Fukui, *J. Phys. Chem.* **74**, 4161 (1970).
- <sup>115</sup> W. Quapp, M. Hirsch, O. Omig, and D. Heidrich, *J. Comput. Chem.* **19**, 1087 (1998).
- <sup>116</sup> M. Hirsch and W. Quapp, *J. Mol. Struct. (Theochem)* **683**, 1 (2004).
- <sup>117</sup> D. Rowe and A. Ryman, *J. Math. Phys.* **23**, 732 (1982).
- <sup>118</sup> D. Hoffman, R. Nord, and K. Reudenberg, *Theor. Chim. Acta* **69**, 265 (1986).
- <sup>119</sup> A. Tachibana, *Theoret. Chim. Acta* **58**, 301 (1981).
- <sup>120</sup> J. Q. Sun and K. Reudenberg, *J. Chem. Phys.* **98**, 9707 (1993).
- <sup>121</sup> R. Zwanzig, *Nonequilibrium Statistical Mechanics* (Oxford University Press, Oxford, 2001).
- <sup>122</sup> J. A. Nummela and B. K. Carpenter, *JACS* **124**, 8512 (2002).
- <sup>123</sup> F. F. Crim, *Fraday Disc.* **157**, 9 (2012).
- <sup>124</sup> D. Schwarzer, J. Troe, M. Votsmeier, and M. Zerezke, *J. Chem. Phys.* **105**, 3121 (1996).
- <sup>125</sup> P. A. Arnold and B. K. Carpenter, *Chem. Phys. Lett.* **328**, 90 (2000).
- <sup>126</sup> D. J. Mann and M. D. Halls, *Phys. Chem. Chem. Phys.* **4**, 5066 (2002).
- <sup>127</sup> W. Quapp, J. M. Bofill, and A. Aguilar-Mogas, *Theor. Chem. Acct* **129**, 803 (2011).
- <sup>128</sup> W. Quapp and J. M. Bofill, *J. Math. Chem.* **50**, 2061 (2012).

$x^*$	$c_1$	$c_2$	$c_3$	$c_4$	$c_5$	$c_6$
2.05	0.622088	0.249578	0.401924	0.0040275	-0.459044	-0.106126
2.0	0.619384	0.318432	0.484549	-0.131496	-0.63717	-0.0986087
2.1	0.625518	0.183133	0.32219	0.136952	-0.286571	-0.111012

TABLE I: Coefficients  $c_k$  for the potential eq. (2.1); sets of coefficients listed correspond to different values of the coordinate  $x^*$  specifying the location of the upper minimum in the potential.

$x^*$	Critical point	$x$	$y$	$E$
2.0 (U)	Upper saddle	0	0	0
	Lower saddle (ridge)	1.983	0.093	-3.969
	Upper minimum	2	1.20	-6.00
	Lower minimum	2.4	-1.20	-7.50
	VRI point	0.508	0.020	-0.647
2.05 (U)	Upper saddle	0	0	0
	Lower saddle (ridge)	1.985	0.097	-3.967
	Upper minimum	2.05	1.20	-6.00
	Lower minimum	2.4	-1.20	-7.50
	VRI point	0.524	0.022	-0.683
2.1 (L)	Upper saddle	0	0	0
	Lower saddle (ridge)	1.987	0.101	-3.964
	Upper minimum	2.1	1.20	-6.00
	Lower minimum	2.4	-1.20	-7.50
	VRI point	0.542	0.025	-0.723

TABLE II: Coordinates  $(x, y)$  and energies  $E$  of critical points of potential eq. (2.1), computed for different values of coordinate  $x^*$ . Coordinates and energies of VRI points are also listed. We indicate whether the IRC initiated at the upper TS terminates at the upper (U) or lower (L) minimum.

## Figure Captions

FIG. 1: (a) Typical reaction profile of two consecutive transition states (T1, T2) linking starting material (S) with the intermediate (I) and product (P). (b) PES featuring a VRI as an alternative mechanistic situation featuring two transition states, but no intermediate. (Fig. 1 of ref. 7.)

FIG. 2: Contour plots of the potentials corresponding to values  $x^* = 2.00$  and  $x^* = 2.10$ , respectively. Also shown are the corresponding IRC paths (blue) connecting the upper TS with one of the 2 product minima. The locations of the saddle points and minima are given in Table II. For each value  $x^* = 2.0$  and  $x^* = 2.1$ , we plot zero contours of the determinant of the Hessian matrix  $\mathcal{H}$  (red) and of the quantity  $\mathbf{g} \cdot \text{adj}[\mathcal{H}] \cdot \mathbf{g}$  (green). Each plot exhibits a single VRI point at the intersection of the 2 contour lines, close to but not actually on the IRC path. Locations and energies of the VRI points are given in Table II.

FIG. 3: (a) Newton trajectories (magenta/green) for the case  $x^* = 2.05$ . The green trajectories are singular trajectories connecting critical points to the VRI point on the potential. (b) Gradient extremal paths (magenta) for the case  $x^* = 2.05$ . At gradient extremal points, the gradient vector  $\mathbf{g}$  is an eigenvector of the Hessian  $\mathcal{H}$ . The IRC (blue) is also included for comparison.

FIG. 4: Trajectory bundles and fractional product yields for  $x^* = 2.0$  and  $x^* = 2.1$  at energy  $E = 0.1$ . No dissipation ( $\gamma = 0$ ).

FIG. 5: Trajectory bundles and fractional product yields for  $x^* = 2.0$  and  $x^* = 2.1$  at energy  $E = 0.01$ . No dissipation ( $\gamma = 0$ ).

FIG. 6: Fractional product yields for (a)  $x^* = 2.0$  and (b)  $x^* = 2.1$  at energy  $E = 0.01$  for times  $0 \leq t \leq t_{\text{max}} = 100$ . The dashed blue line shows the cumulative fraction of trajectories recrossing the upper DS.

FIG. 7: Trajectory bundles and fractional product yields for  $x^* = 2.0$  and  $x^* = 2.1$ . Initial energy  $E = 0.01$ , dissipation parameter  $\gamma = 0.5$ .

FIG. 8: Trajectory bundles and fractional product yields for  $x^* = 2.0$  and  $x^* = 2.1$ . Initial energy  $E = 0.01$ , dissipation parameter  $\gamma = 0.25$ .

FIG. 9: Fraction of trajectories in the lower well versus dissipation parameter  $\gamma$ . (a)  $x^* = 2.0$ ,  $E = 0.01$ ; (b)  $x^* = 2.05$ ,  $E = 0.01$ ; (c)  $x^* = 2.1$ ,  $E = 0.01$ ; (d)  $x^* = 2.05$ ,  $E = 0.1$ .

FIG. 10: Time-dependent fractional product yields and trajectory segments,  $t_1 \leq t \leq t_2$ ,  $t_1 = 8.5$ ,  $t_2 = 9.0$ ,  $x^* = 2.05$ , initial energy  $E = 0.01$ . (a) Trajectory segments,  $\gamma = 0.13$ ; (b) Fractional yield vs  $t$ ,  $\gamma = 0.13$ ; (c) Trajectory segments,  $\gamma = 0.1$ ; (d) Fractional yield vs  $t$ ,  $\gamma = 0.1$ .

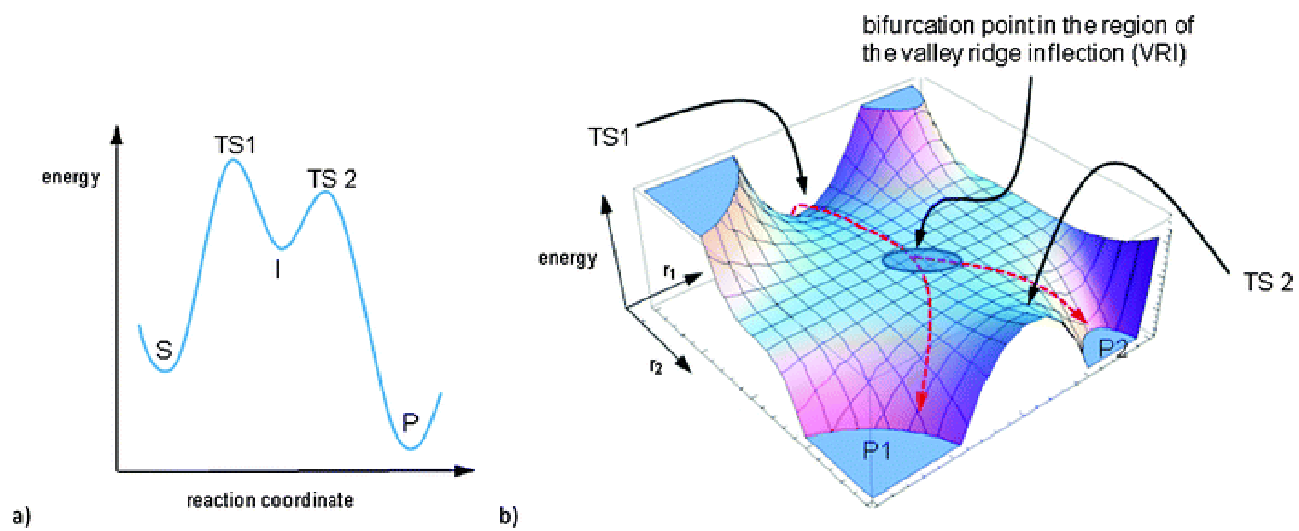


FIGURE 1



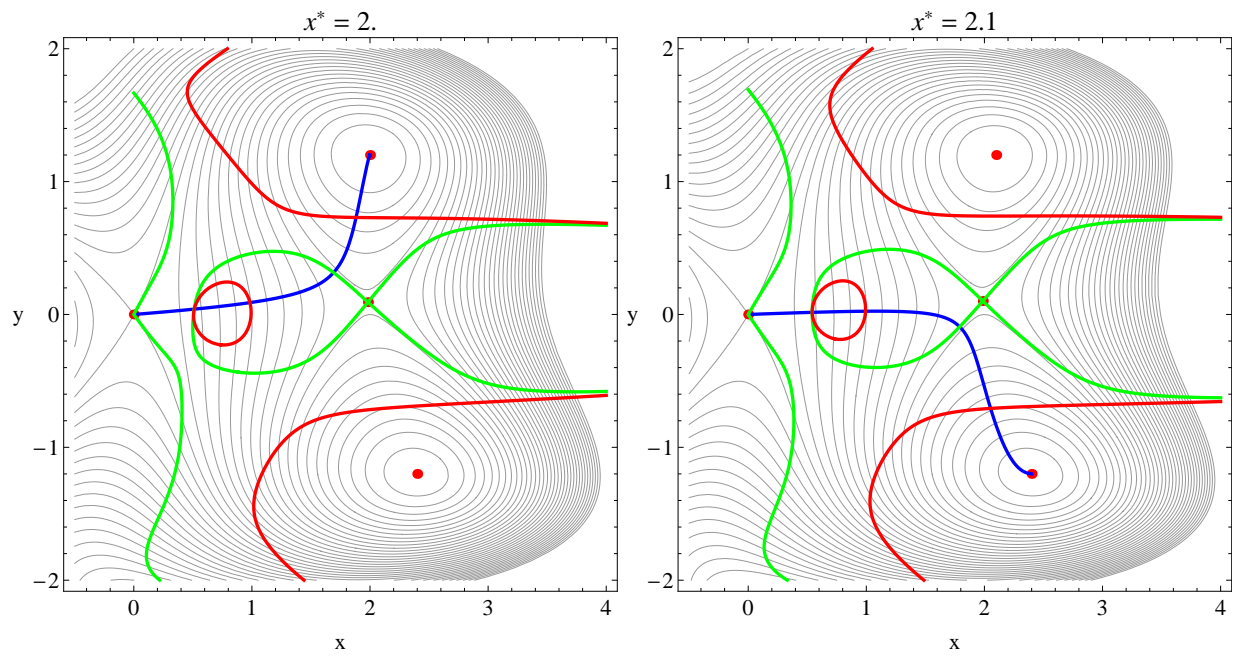


FIGURE 2

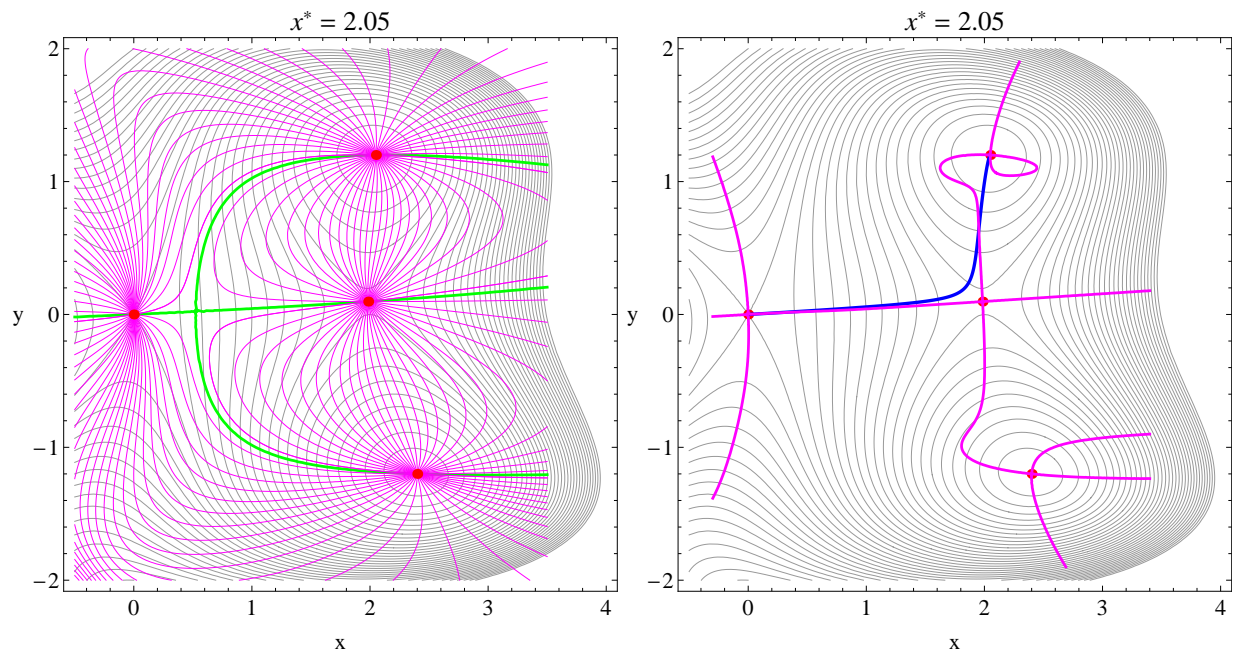


FIGURE 3

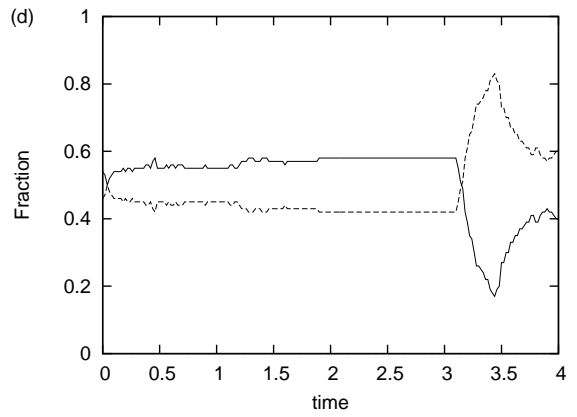
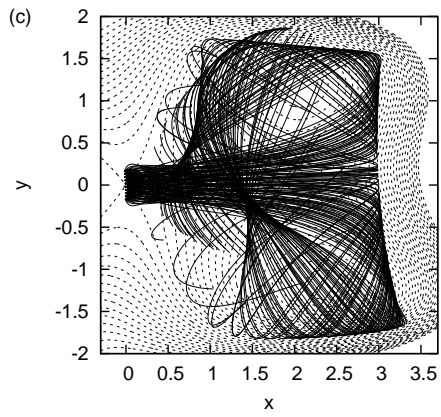
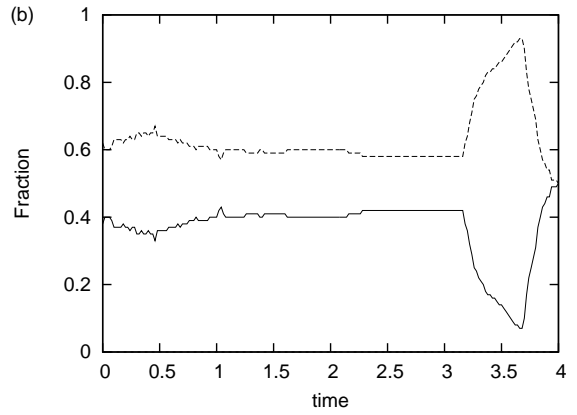
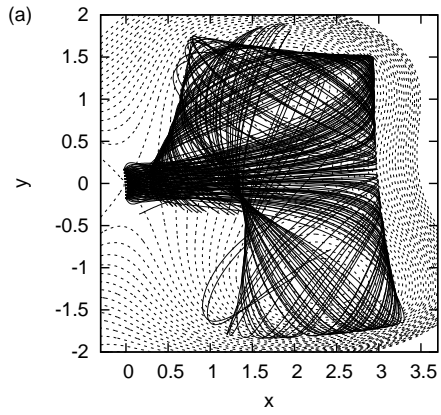


FIGURE 4

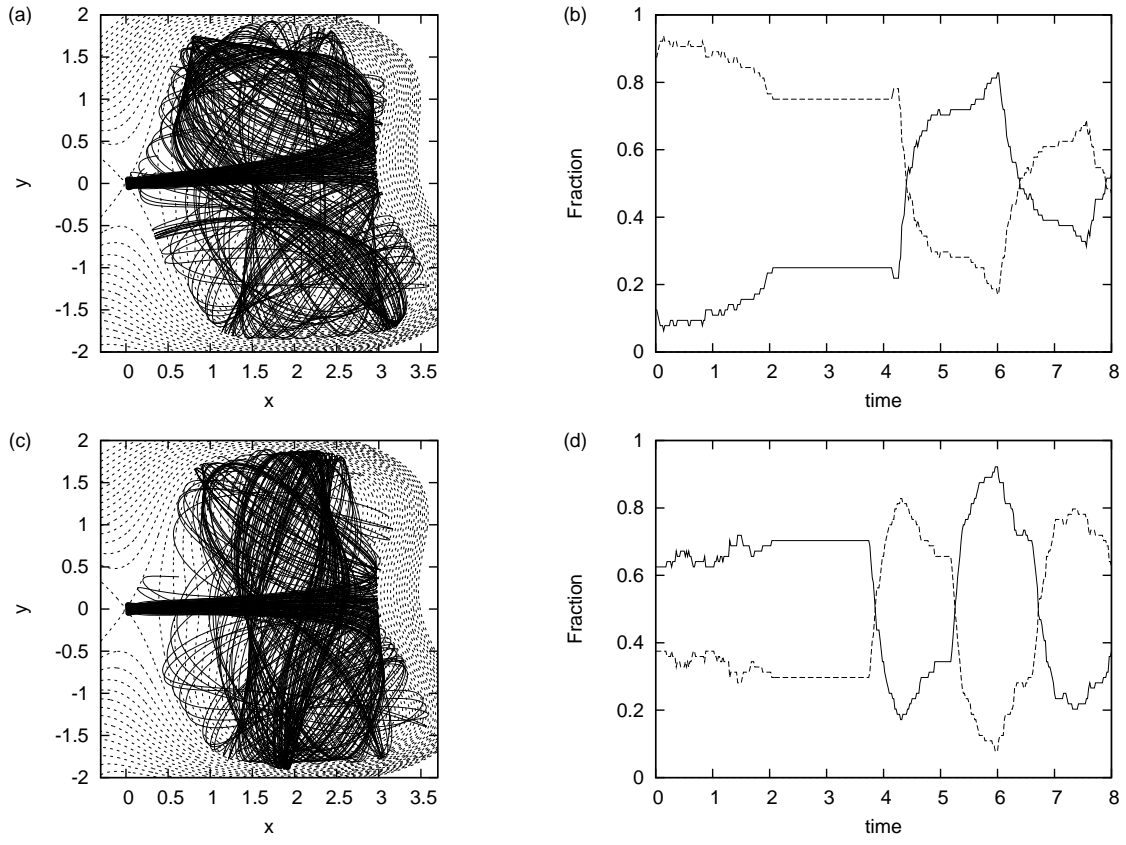


FIGURE 5

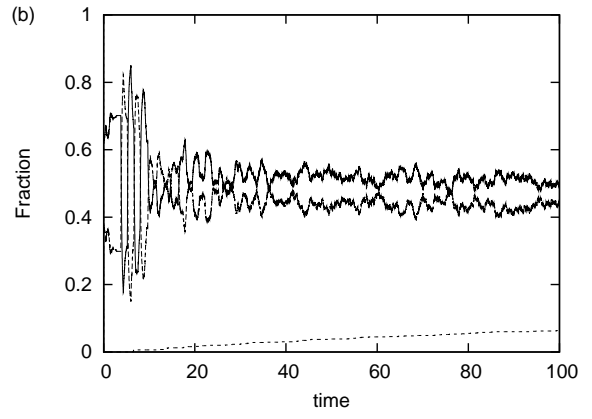
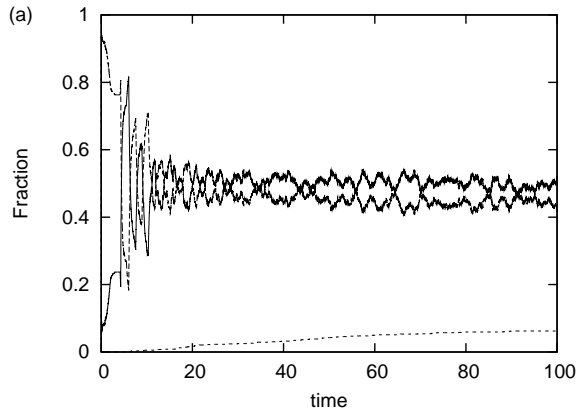


FIGURE 6

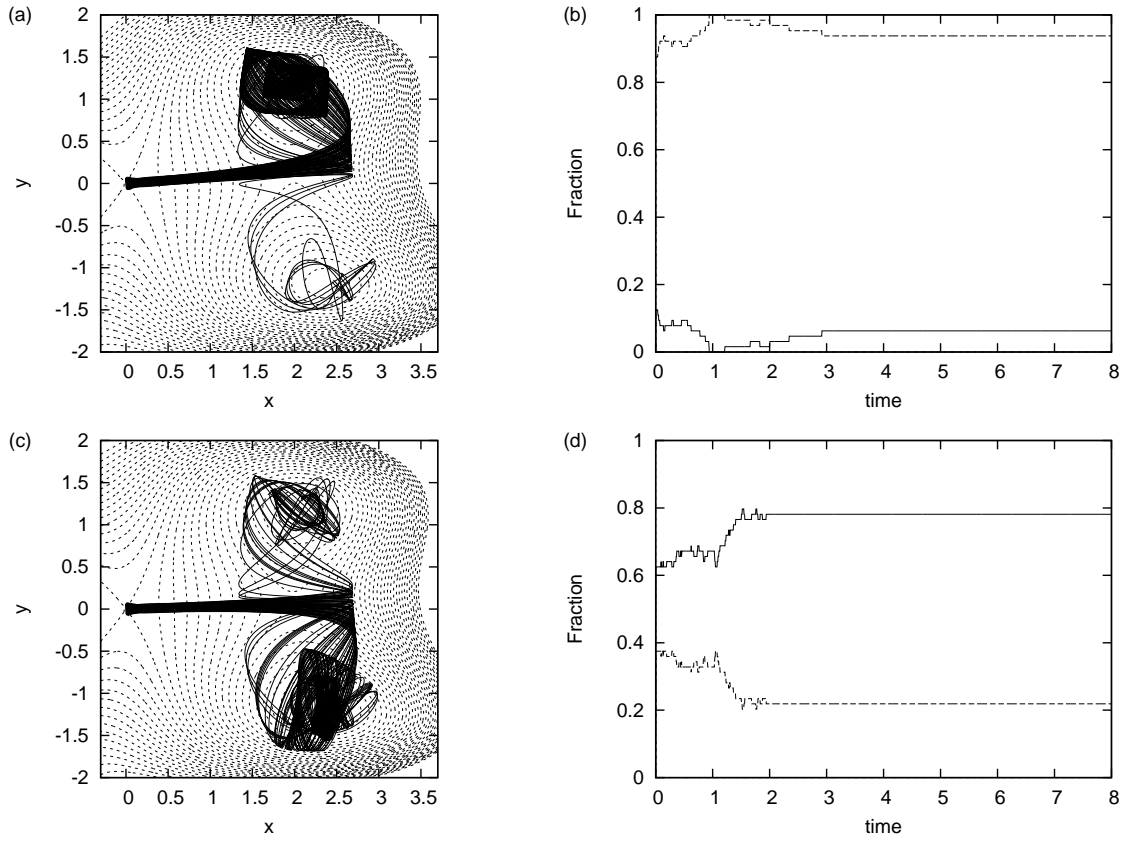


FIGURE 7

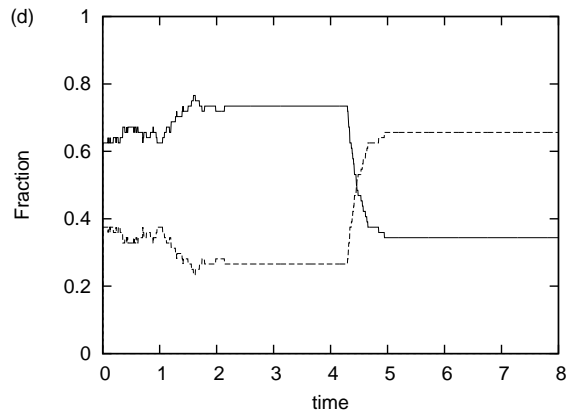
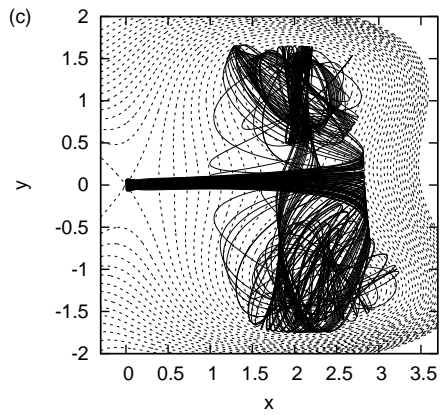
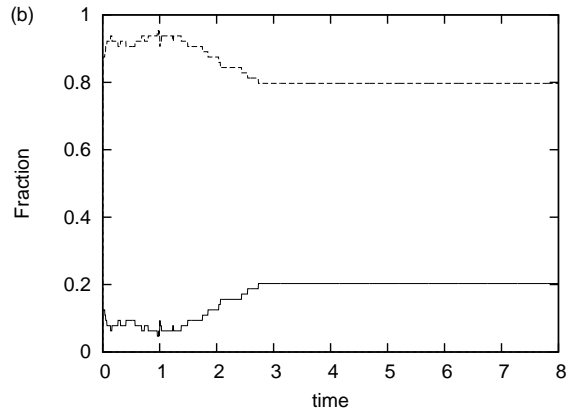
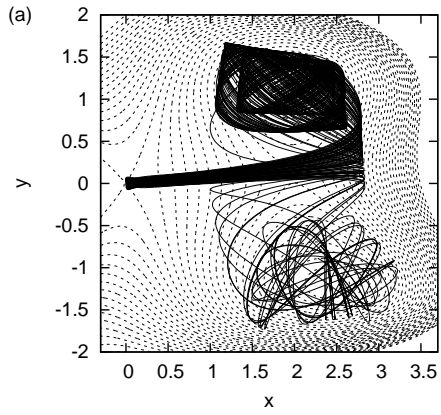


FIGURE 8

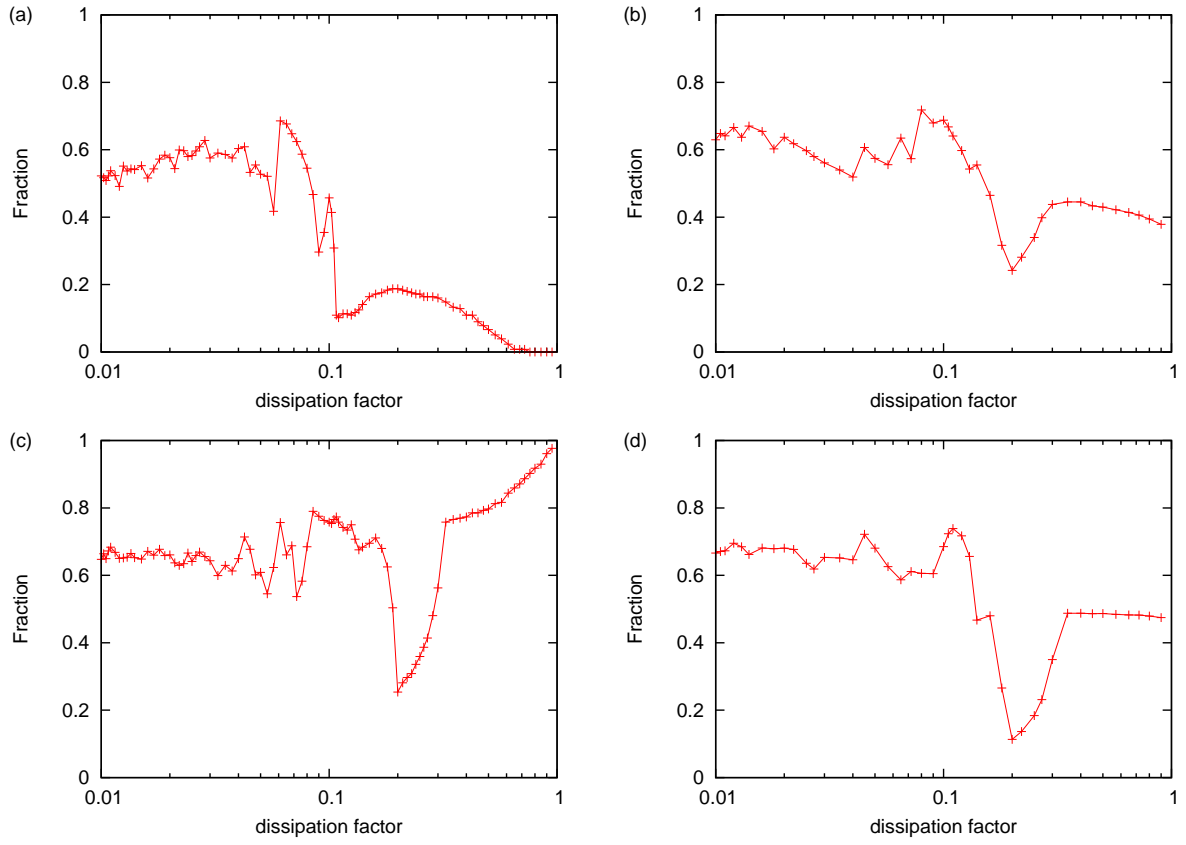


FIGURE 9



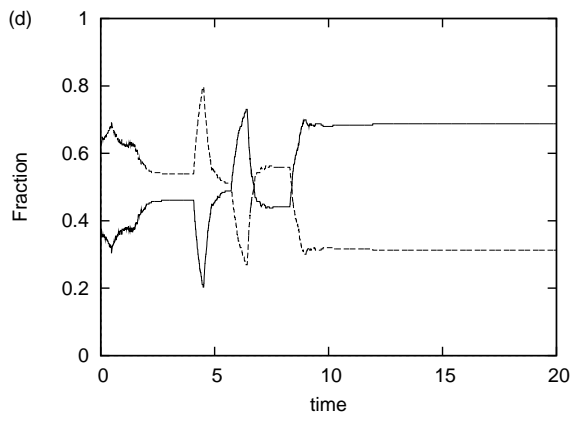
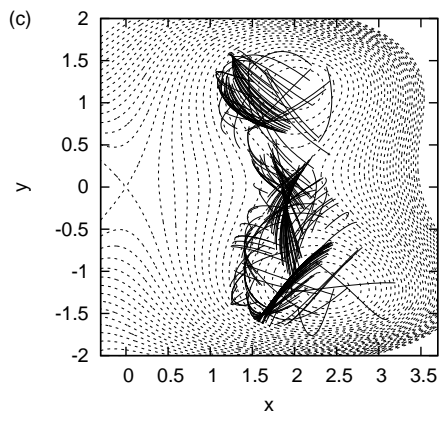
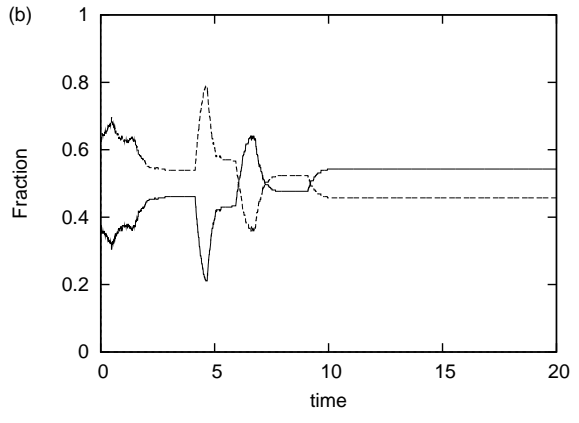
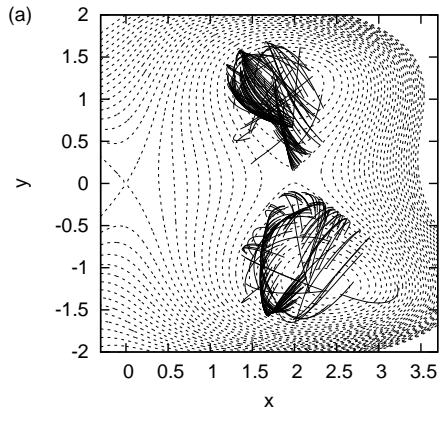


FIGURE 10